# Electronic Supplementary Information

**Accurate, Hysteresis-Free Temperature Sensor for Health Monitoring Using a Magnetic Sensor and Pristine Polymer**

*Wooseong Jeong, Mijin Kim, Jae-Hyun Ha, Nora Asyikin Binti Zulkifli, Jung-Il Hong, CheolGi Kim, and Sungwon Lee**

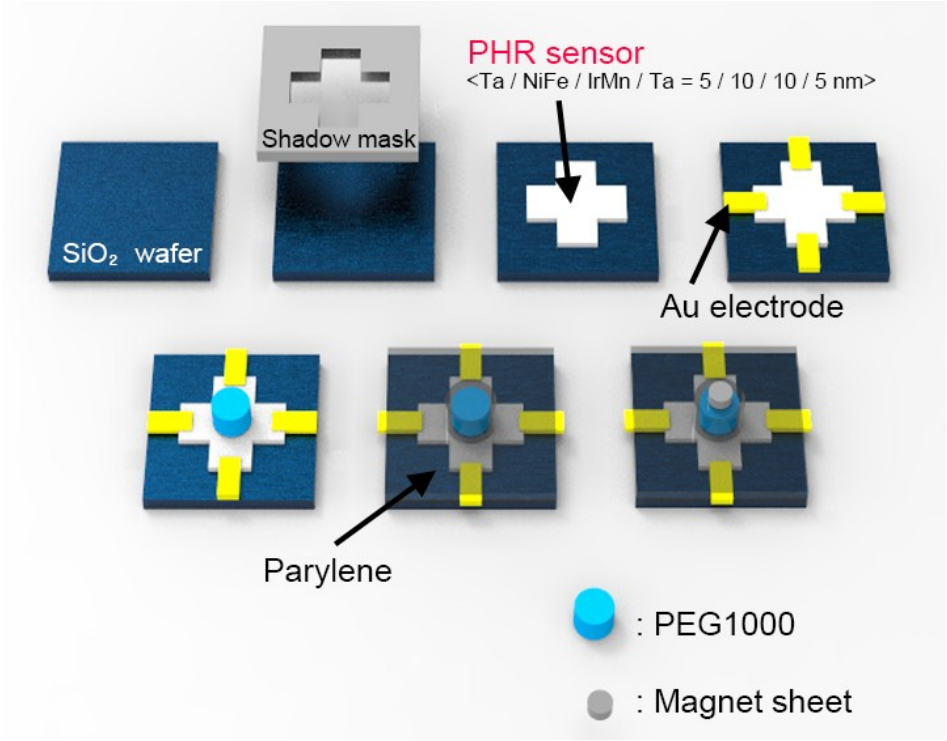


**Fig. S1** Fabrication process. The planar Hall resistance (PHR) sensor and the Au electrode layers were sputtered using shadow masks.

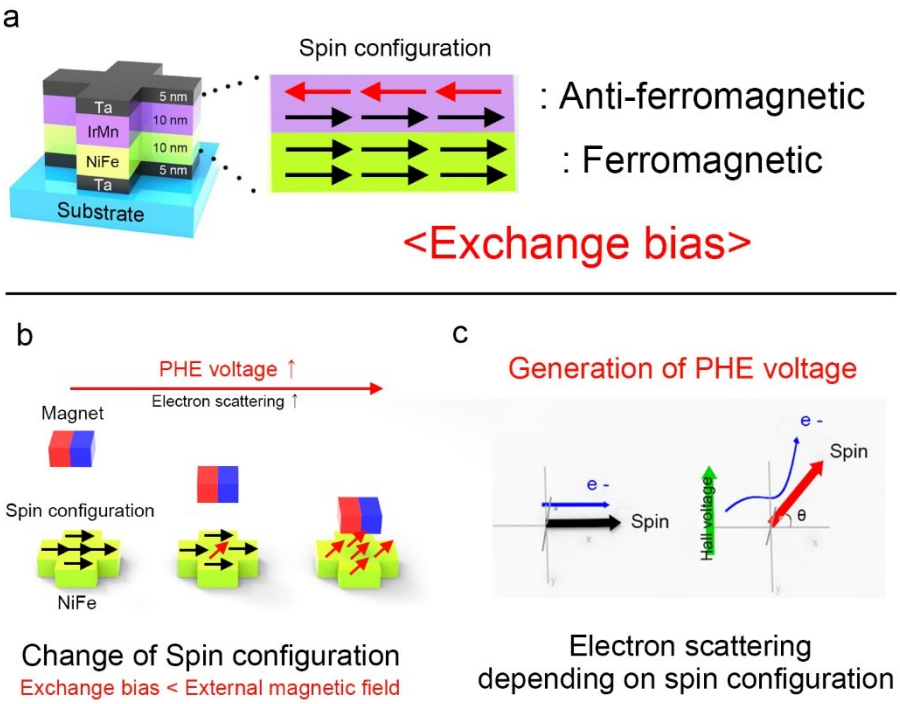


**Fig. S2** Principles of the planar Hall effect (PHE) voltage. (a) Spin configuration of the PHR sensor layers. (b) Spin configuration of the PHR sensor layers depending on the distance between the PHR sensor and the magnet when a magnetic field is applied. (c) Generation of PHE voltage in accordance with the anomalous Hall effect.

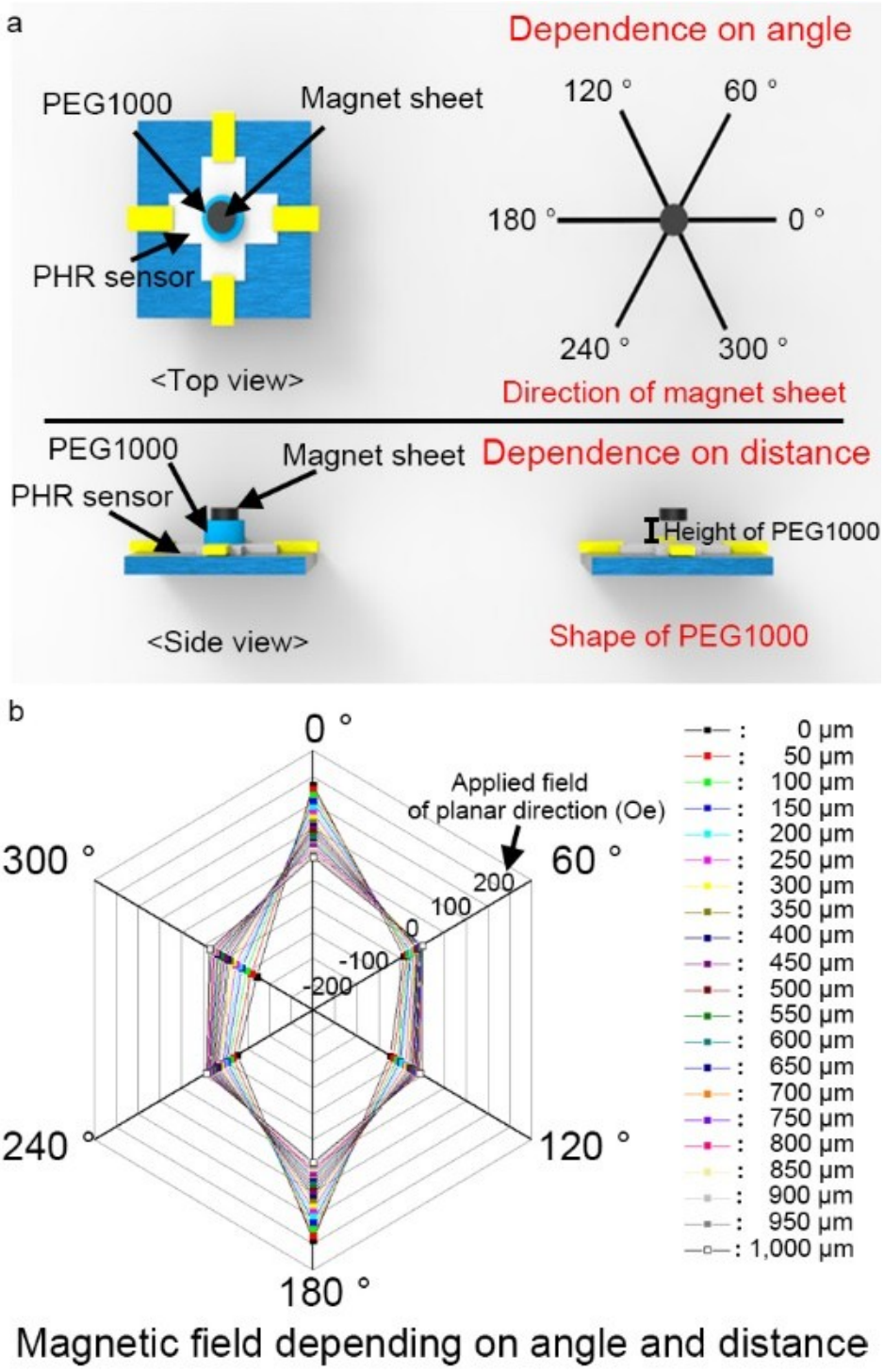


**Fig. S3** Magnetic characteristics of the anisotropic magnet sheet. (a) Schematic diagram of the distance and angular dependence of the magnetic sheet. (b) Magnetic field strength depending on the distance and the angle.

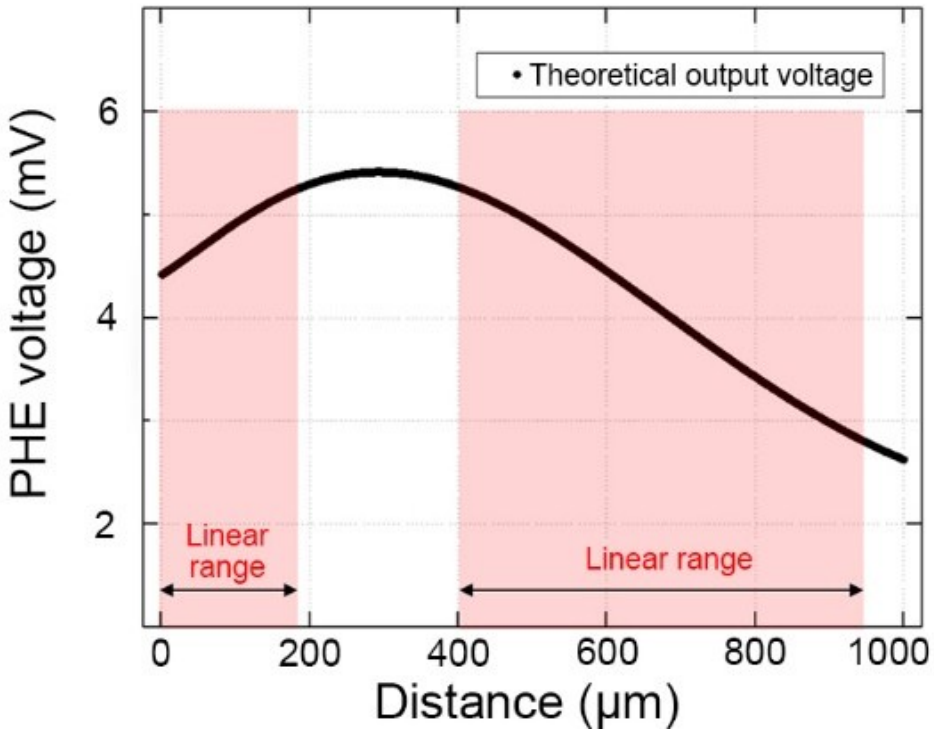


**Fig. S4** Theoretical PHE voltage as a function of the distance between the PHR sensor and the magnet sheet calculated from Fig. 2c and 2d. The height of the polymer layer can be manipulated during molding.

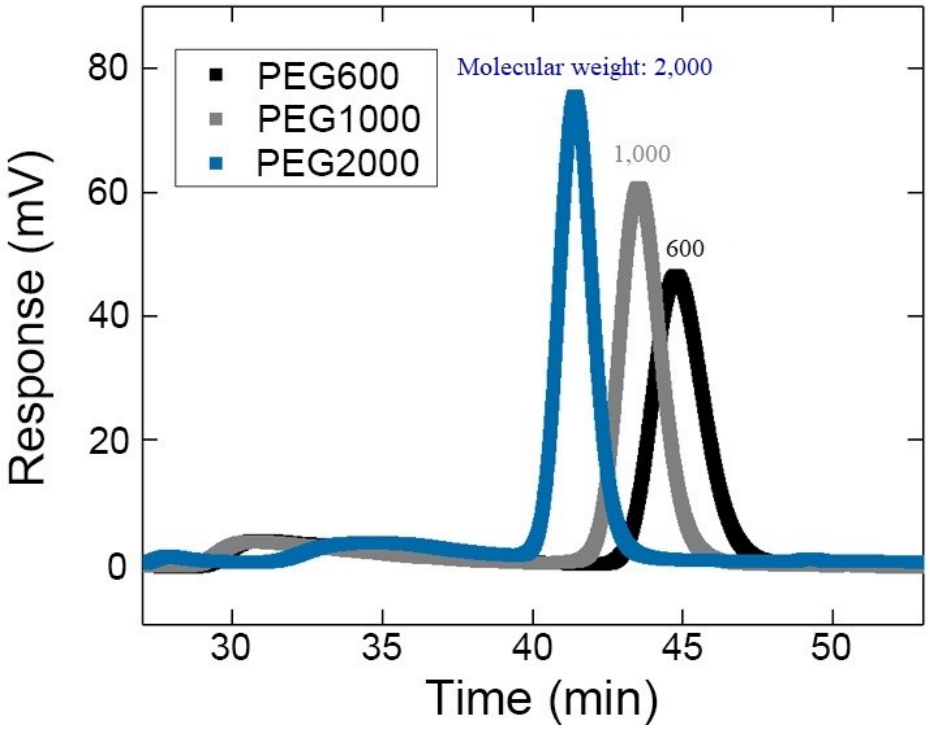


**Fig. S5** GPC (Gel permeation chromatography) curves showing the molecular weight distributions of PEG600, PEG1000 and PEG2000

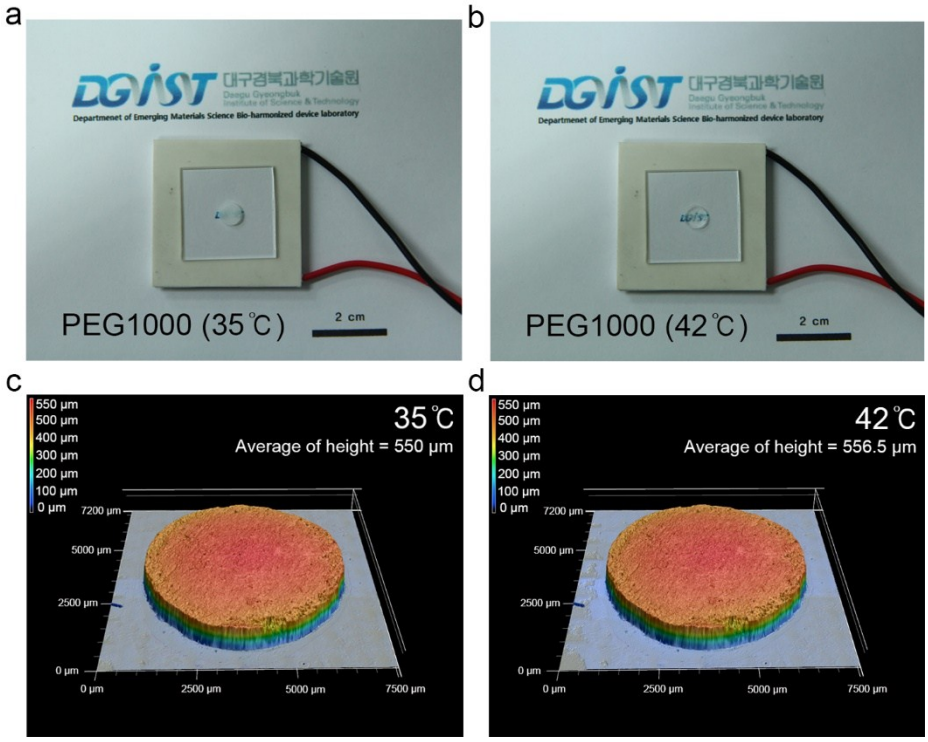


**Fig. S6** Images of molded PEG1000. (a, b) Photographs (scale bar = 2 cm) and (c, d) 3D structural images of the molded PEG1000 at 35 and 42 °C, respectively.

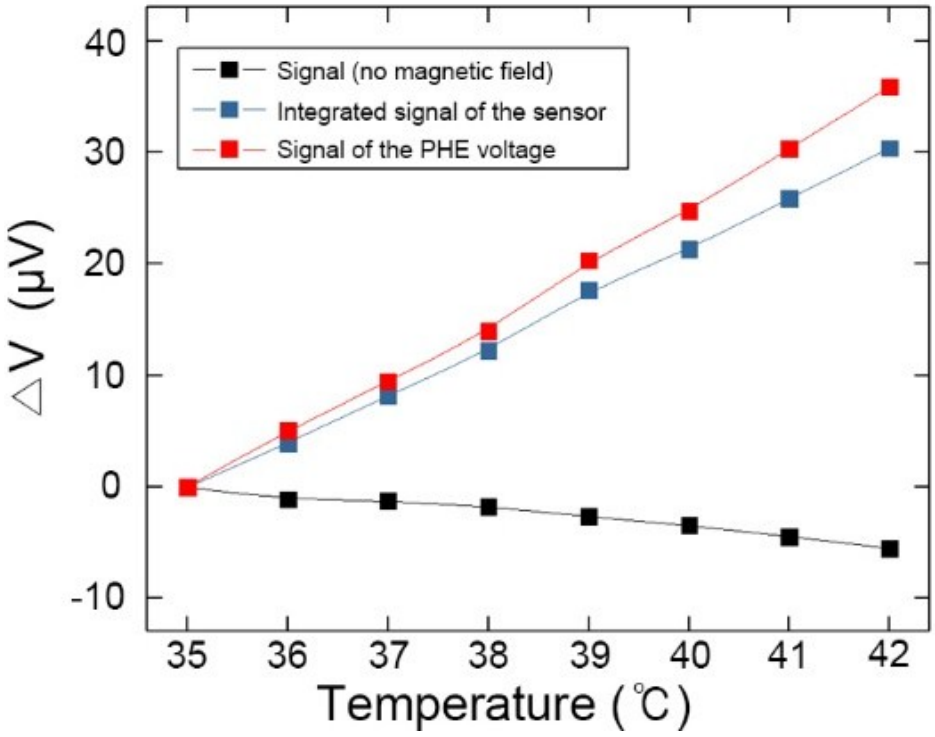


**Fig. S7** Output voltage of the temperature sensor depending on the sensor layers and the PHE voltage as a function of temperature.

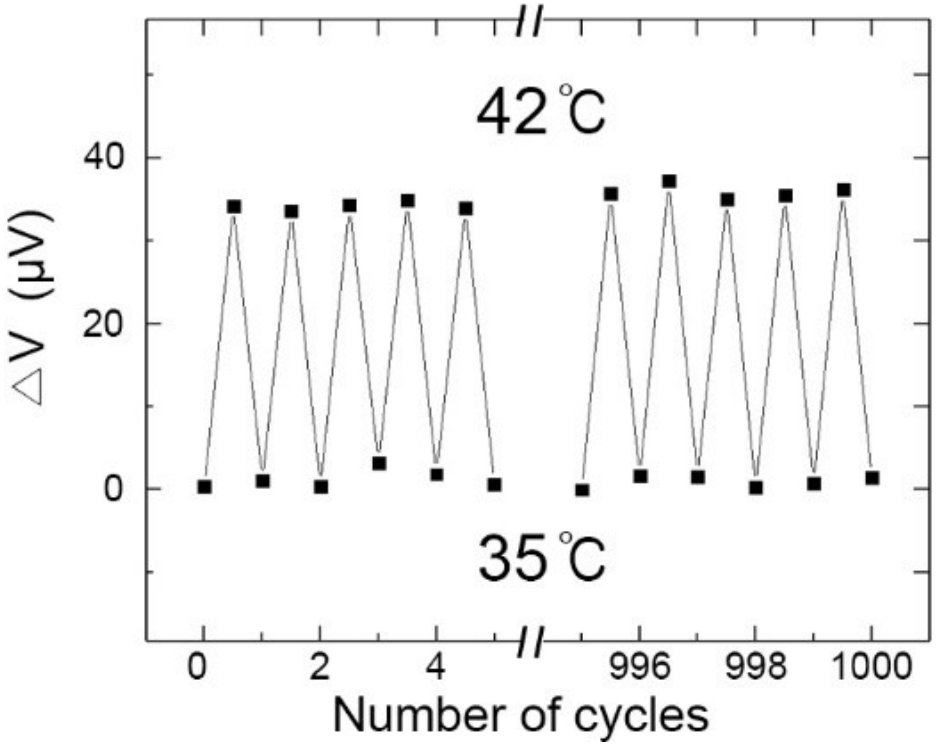


**Fig. S8** Output voltage during initial and final 5 s of the cycling test between 35 and 42 °C.

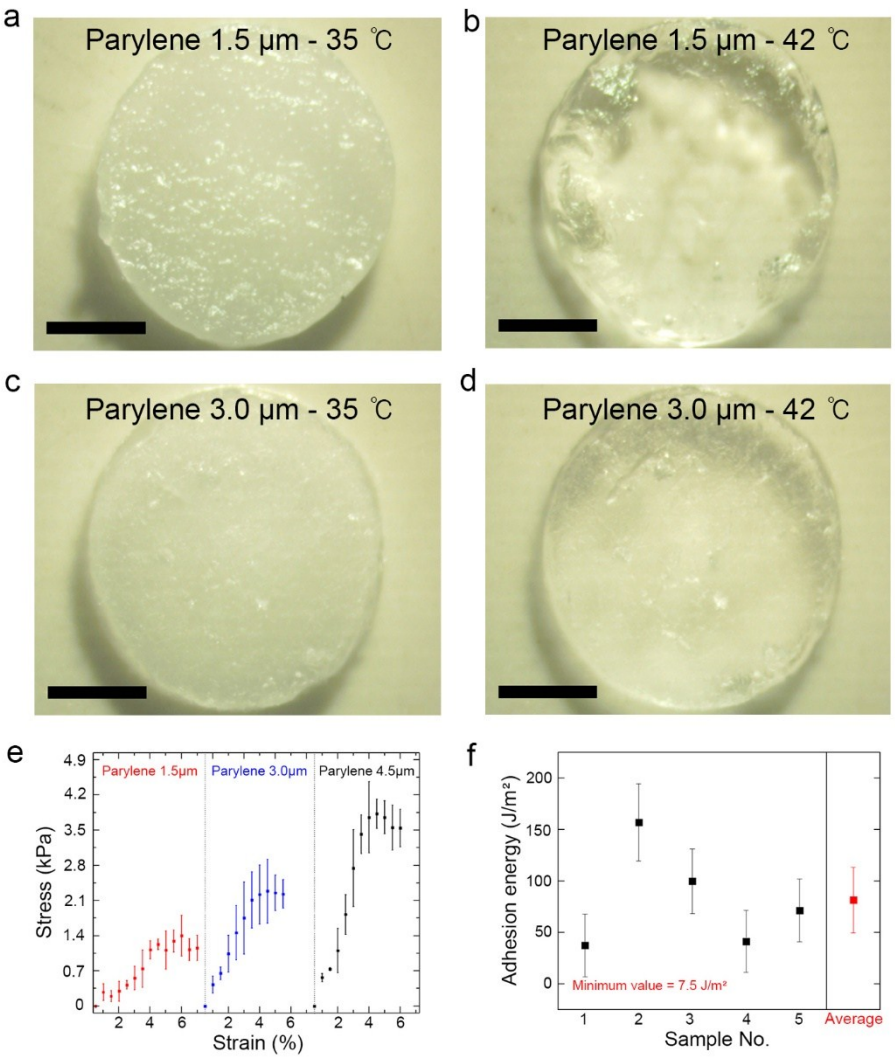


**Fig. S9** Physical characteristics of the polymeric system. Physical appearance of the molded PEG1000 with (a, b) 1.5-μm-thick Parylene films at 35 and 42 °C, respectively and (c, d) 3.0 μm-thick Parylene films at 35 and 42 °C, respectively (scale bars = 2 mm). (e) Stress–strain curves of 1.5-, 3.0-, and 4.5-μm-thick Parylene films. (f) Average adhesion fracture energy between the PHR sensor and Parylene film.

We hypothesized that the Parylene encapsulation layer must satisfy the following two conditions. First, to suitably contain the polymer, the Parylene layer must be able to withstand expansion during heating. Failure to withstand volume changes would result in the deterioration of the Parylene layer. Hence, the mechanical strength of the Parylene film must be high enough to withstand the stress applied by the expansion. We prepared two polymeric systems overlaid with either a 1.5- or 3.0-μm-thick Parylene film. The 1.5-μm-thick Parylene

film could not maintain the shape of the polymer (Fig. S8a and 8b), whereas the 3.0-μm-thick Parylene layer was clearly able to withstand the expansion energy (Fig. S8c and 8d).

Second, to ensure reversible volume expansion, the adhesion energy between the Parylene layer and PHR sensor must be higher than the expansion energy to avoid delamination. The separation of the Parylene layer and PHR sensor would allow the polymer to expand along the *x*- and *z*-axes as well as the *y*-axis, meaning that its shape could not be maintained, and the repeatability of the measurements would be poor. The expansion and adhesion energies were therefore calculated and compared. The expansion energy was theoretically calculated from the minimum thickness of the Parylene layer necessary to endure the expansion (3.0 μm, Fig. S8), surface area (38.29 $\mu m^2$), height variation (6.5 μm between 35 and 42 °C) of the molded PEG1000, and the maximum force applied to the Parylene film, which was calculated with regard to the thickness using stress–strain curves measured with a universal testing machine (UTM) (Fig. S8e). The expansion energy was calculated to be 0.49–1.95 $mJ \cdot m^{-2}$.

The adhesion energy between the PHR sensor and the Parylene film was calculated using the following equation:

$$G_{ic} = (P_f/b)(1 - \cos\theta), \quad \text{(S1)}$$

where $G_{ic}$ is the adhesion fracture energy, $P_f$ is the peeling force, $b$ is the length of the adhesion line, and $\theta$ is the peeling angle between layers. $P_f$ was calculated by performing a peel test in the UTM, and $P_f$, $b$, and $\theta$ were easily measured when fabricating and testing the sample. The range of average adhesion energies was approximately 50–115 $J \cdot m^{-2}$, with a minimum value of 7.5 $J \cdot m^{-2}$ (Fig. S8f).

When comparing the expansion and adhesion energies, the maximum expansion energy (1.95 $mJ \cdot m^{-2}$) and minimum adhesion energy (7.5 $J \cdot m^{-2}$) were used to ensure that delamination would not occur even in the "worst-case" scenario. Even at these extremes, the expansion energy was almost three orders of magnitude lower than the adhesion energy. Therefore, our sensor not only can reversibly accommodate thermal volume expansion but

also can restrict such expansion to be only along the *y*-axis, thus effectively maximizing the sensitivity.